VECTOR-QUANTIZED IMAGE MODELING WITH IMPROVED VQGAN

Jiahui Yu Xin Li Jing Yu Koh Han Zhang Ruoming Pang James Qin Alexander Ku Yuanzhong Xu Jason Baldridge Yonghui Wu
Google Research
jiahuiyu@google.com

ABSTRACT

Pretraining language models with next-token prediction on massive text corpora has delivered phenomenal zero-shot, few-shot, transfer learning and multi-tasking capabilities on both generative and discriminative language tasks. Motivated by this success, we explore a Vector-quantized Image Modeling (**VIM**) approach that involves pretraining a Transformer to predict rasterized image tokens autoregressively. The discrete image tokens are encoded from a learned Vision-Transformer-based VQGAN (**ViT-VQGAN**). We first propose multiple improvements over vanilla VQGAN from architecture to codebook learning, yielding better efficiency and reconstruction fidelity. The improved ViT-VQGAN further improves vector-quantized image modeling tasks, including unconditional, class-conditioned image generation and unsupervised representation learning. When trained on ImageNet at 256×256 resolution, we achieve Inception Score (IS) of 175.1 and Fréchet Inception Distance (FID) of 4.17, a dramatic improvement over the vanilla VQGAN, which obtains 70.6 and 17.04 for IS and FID, respectively. Based on ViT-VQGAN and unsupervised pretraining, we further evaluate the pretrained Transformer by averaging intermediate features, similar to Image GPT (iGPT). This ImageNet-pretrained VIM-L significantly beats iGPT-L on linear-probe accuracy from 60.3% to 73.2% for a similar model size. VIM-L also outperforms iGPT-XL which is trained with extra web image data and larger model size.

1 INTRODUCTION

Natural language processing (NLP) has recently experienced dramatic improvements from learning general-purpose representations by pretraining language models on unlabeled text corpora. This strategy has produced large performance gains for a wide range of natural language generation (NLG) and natural language understanding (NLU) tasks (Dai & Le, 2015; Radford et al., 2018; 2019; Brown et al., 2020). Conceptually, generative pretraining models the data density $P(X)$ in a tractable way, with the hope of also helping discriminative tasks of $P(Y|X)$ (Lasserre et al., 2006); importantly, there are no limitations on whether the signals are from the language domain or others, such as vision.

In computer vision, in contrast, most recent unsupervised or self-supervised learning research focuses on applying different random augmentations to images, with the pretraining objective to distinguish image instances (Chen et al., 2020b; He et al., 2020; Chen et al., 2020d; Grill et al., 2020; Chen et al., 2020c; Caron et al., 2021). The quality of learned representation relies on manually chosen augmentations, such as random brightness, cropping, blurring, and others. Chen et al. (2020a) explored GPT-style (Radford et al., 2018) generative pretraining on images by autoregressively predicting pixels without incorporating knowledge of the 2D structure. Each pixel is represented as a 9-bit value created by clustering (R, G, B) pixel values, using k-means with k=512. Unfortunately, this color encoding does not scale to typical image resolutions as it entails very long sequences to represent the image (*e.g.*, 224×224 resolution leads to 50,176 tokens per image), and this demands much more memory and computation for training, compared to language models. As a result, iGPT's maximum resolution is 64×64 for image recognition at scale—which severely limits its representation capabilities.

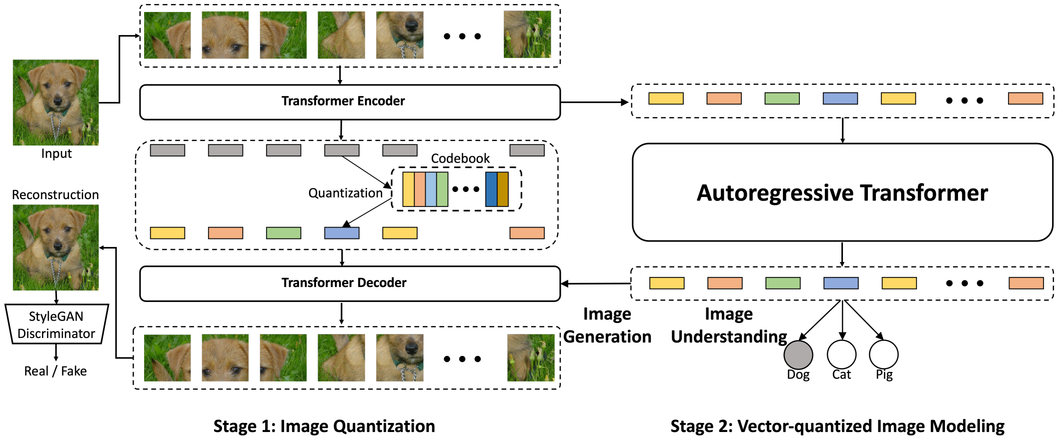

Figure 1: Overview of ViT-VQGAN (left) and Vector-quantized Image Modeling (right) for both image generation and image understanding.

Remarkable image generation results have been achieved by pre-quantizing images into discrete latent variables and modeling them autoregressively, including VQVAE (Oord et al., 2017), DALL-E (Ramesh et al., 2021) and VQGAN (Esser et al., 2021). In these approaches, a convolution neural network (CNN) is learned to auto-encode an image and a second stage CNN or Transformer is learned to model the density of encoded latent variables. These have been proved effective for image generation, but few studies have evaluated the learned representation in discriminative tasks (Ramesh et al., 2021; Esser et al., 2021).

We explore an approach we refer to as Vector-quantized Image Modeling (VIM) and apply it to both image generation and image understanding tasks. VIM follows a two-stage approach:

- **Stage 1: Image Quantization.** Given an image of resolution 256×256, a Vision-Transformer-based VQGAN encodes it into 32×32 discretized latent codes where the codebook size is 8192. We propose multiple improvements–from architecture to codebook learning–to VQGAN (Esser et al., 2021). The resulting ViT-VQGAN is more efficient and improves reconstruction fidelity in terms of pixel-wise reconstruction metrics, Inception Score (IS) and Fréchet Inception Distance (FID). ViT-VQGAN is trained end-to-end on image-only data with combined objective functions of logit-laplace loss, ℓ_2 loss, adversarial loss and perceptual loss (Johnson et al., 2016; Zhang et al., 2018).
- **Stage 2: Vector-quantized Image Modeling.** We train a Transformer model to predict rasterized $32 \times 32 = 1024$ image tokens autoregressively, where image tokens are encoded by a learned Stage 1 ViT-VQGAN. For unconditional image synthesis or unsupervised learning, we pretrain a decoder-only Transformer model to predict the next token. For class-conditioned image synthesis, a class-id token is prepended before the image tokens. To evaluate the quality of unsupervised learning, we average the intermediate Transformer features and learn a linear head to predict the logit of the classes (*a.k.a.*, linear-probe).

We show that one key component for improving both image generation and image understanding with VIM is to have a better image quantizer with respect to both computational efficiency and reconstruction quality. An efficient quantizer can speed up Stage 2 training, where random augmentations are applied first to an image, followed by the encoder of image quantizer to obtain the input tokens. Moreover, an image quantizer with better reconstruction quality can reduce information loss compared with the original image in pixel space, which is critical for image understanding tasks.

The evaluations of our proposed ViT-VQGAN and VIM are studied with three aspects. (1) We evaluate the image quantizer based on reconstruction quality metrics including ℓ_1 distance, ℓ_2 distance, log-laplace distance, as well as Inception Score (IS) and Fréchet Inception Distance (FID) of reconstructed images. (2) We evaluate the capabilities of the learned quantizer for unconditional or class-conditioned image synthesis based on FID and IS, and compare with other methods. (3) We rely on linear-probe accuracy to evaluate representations with the common intuition that good features should linearly separate the classes of downstream tasks.

2 Related Work

Image Synthesis. Image generation has received much attention with the progress of deep generative models, including Generative Adversarial Networks (GANs) (Goodfellow et al., 2014; Zhang et al., 2019b), Variational Autoencoders (VAEs) (Kingma & Welling, 2014; Vahdat & Kautz, 2020), Diffusion Models (Song & Ermon, 2019; Dhariwal & Nichol, 2021) and Autoregressive Models (van den Oord et al., 2016; Parmar et al., 2018). Unlike many autogressive methods which generate sequence directly in pixel space, VQVAE (van den Oord et al., 2017; Razavi et al., 2019) decomposes the image generation process into two stages: the first stage trains a vector quantized autoencoder with image reconstruction objective to convert an image into a shorter sequence of discrete tokens. Then the second stage learns an autoregressive model, e.g., PixelSNAIL (Chen et al., 2018), to model the underlying distribution of token sequences. Driven by the effectiveness of VQVAE and progress in sequence modeling (Vaswani et al., 2017; Devlin et al., 2019), many approaches follow the two-stage paradigm. DALL-E (Ramesh et al., 2021) improves token prediction in second stage by using Transformers (Vaswani et al., 2017), resulting in a strong text-to-image synthesis model. VQGAN (Esser et al., 2021) further uses adversarial loss and perceptual loss (Johnson et al., 2016; Zhang et al., 2018) to train a better autoencoder in the first stage to synthesize greater detail in images.

Image Recognition with Generative Pretraining. Many image generation models (Goodfellow et al., 2014; Kingma & Welling, 2014; Radford et al., 2016; Donahue et al., 2017; Higgins et al., 2017) have been studied for their capabilities in representation learning. However, their performance is usually not superior to competing self-supervised approaches that solve auxiliary classification tasks (Noroozi & Favaro, 2016a; Gidaris et al., 2018a; van den Oord et al., 2018). BigBiGAN (Donahue & Simonyan, 2019a) first demonstrated that a generation-based model can match other self-supervised methods in representation learning on ImageNet. iGPT (Chen et al., 2020a) uses the autoregressive objective to learn a giant transformer that directly predicts pixel values, producing even more competitive results. Compared to iGPT, our method first tokenizes the original image into discrete image tokens and then trains a transformer to predict them. As a result, our approach obtains comparable results with smaller model and less data. Similar to our method in predicting image tokens, BEiT (Bao et al., 2021) follows pre-training scheme of BERT Devlin et al. (2019) by learning to recover randomly masked image tokens with a bidirectional transformer. Unlike BEiT, we explore vector-quantized image modeling for image generation in addition to image recognition.

3 Vector-quantized Images with ViT-VQGAN

The Vector-quantized Variational AutoEncoder (VQVAE) (van den Oord et al., 2017) is a CNN-based auto-encoder whose latent space is a matrix of discrete learnable variables, trained end-to-end via straight-through estimation. Esser et al. (2021) introduce VQGAN, a model which improves upon VQVAE by introducing an adversarial loss produced by a discriminator. Below, we introduce further improvements to VQGAN that boost efficiency and enhance reconstruction quality.

3.1 VQGAN with Vision Transformers

The core network architectures used by both VQVAE and VQGAN to encode and reconstruct images are CNNs. VQGAN introduces transformer-like elements in the form of non-local attention block (Zhang et al., 2019a), allowing it to capture distant interactions with fewer layers. We propose taking this approach one step further by replacing the CNN encoder and decoder with Vision Transformer (ViT) (Dosovitskiy et al., 2020), as shown in Figure 1. Given sufficient data (for which unlabeled image data is plentiful) we find that ViT-VQGAN is less constrained by the inductive priors imposed by convolutions. Furthermore, ViT-VQGAN yields better computational efficiency on accelerators, and produces higher quality reconstructions, as shown in Table 1.

The encoder of ViT-VQGAN first maps 8×8 non-overlapping image patches into image tokens, followed by Transformer blocks, encoding a 256×256 resolution image into a $32\times32=1024$ token sequence. The decoder performs the inverse operation, mapping each image token from latent variables back to 8×8 image patches and regrouping them into a 256×256 image (see Figure 1). At the output of transformer blocks, we apply a two-layer feed-forward network with a tanh activation layer

Architecture	Model Size (encoder-decoder)	Throughput ↑ (imgs/sec)	ℓ_2 loss ↓ (1e-2)	Logit-Laplace loss ↓	FID ↓	IS ↑
ViT-VQGAN	Small-Small	**1520**	3.34	-2.44	1.99	184.4
CNN-VQGAN	Channels × 1	946	3.81	-2.36	2.26	178.7
ViT-VQGAN	Base-Base	960	**3.09**	**-2.54**	**1.55**	**190.2**
CNN-VQGAN	Channels × 2	400	3.44	-2.46	1.91	183.4
ViT-VQGAN	Small-Large	384	**2.88**	**-2.58**	**1.28**	**192.3**

Table 1: ViT-VQGAN achieves better speed-quality trade-offs compared with CNN-VQGAN. This in turn further speeds up Stage 2 training. Throughputs are benchmarked with the same 128 CloudTPUv4 devices.

in the middle. No activation is applied at the output of ViT-VQGAN encoder or decoder. We find that this simple approach yields high quality reconstructions without any noticeable grid artifacts.

3.2 Codebook Learning

Vanilla VQVAEs usually suffer from low codebook usage due to the poor initialization of the codebook. Therefore, during training a significant portion of codes are rarely used, or *dead*. The reduction in effective codebook size results in worse reconstructions in stage 1 quantizer training and poor diversity in stage 2 for image synthesis. As a result, VQGAN (Esser et al., 2021) relies on top-k and top-p (nucleus) sampling heuristics (Holtzman et al., 2020) with a default codebook size of 1024 to obtain best results for image synthesis. We propose two improvements that can significantly encourage the codebook usage even with a larger codebook size of 8192. During image synthesis, we perform simple sampling with temperature of 1.0 without top-k and top-p heuristics.

The training objective of vector-quantization is defined as follows:

$$L_{\text{VQ}} = \|\text{sg}[z_e(x)] - e\|_2^2 + \beta \|z_e(x) - \text{sg}[e]\|_2^2. \tag{1}$$

Here, $\text{sg}(x) \equiv x$, $\frac{\mathrm{d}}{\mathrm{d}x}\text{sg}(x) \equiv 0$ is the stop-gradient operator, β is a commitment loss hyperparameter set to 0.25 in all our experiments, and e is the codebook vector. The quantized codebook index is determined by looking up the codebook vector closest to the input features $z_e(x)$ in terms of the Euclidean distance, yielding $i = \text{argmin}_j \|z_e(x) - e_j\|_2^2$.

Factorized codes. We introduce a linear projection from the output of the encoder to a low-dimensional latent variable space for code index lookup (*e.g.*, reduced from a 768-d vector to a 32-d or 8-d vector per code) and find it has an immediate boost of codebook usage. The factorization can be viewed as decoupling code lookup and code embedding: we lookup the the closest variable encoded from input on a lower-dimensional lookup space and then project the matched latent code to the high-dimensional embedding space. Our experiments show reducing dimension of lookup space from 256-d to 32-d consistently improves reconstruction quality. A detailed illustration is provided in the supplementary materials.

ℓ_2-normalized codes. We also apply ℓ_2 normalization on the encoded latent variables $z_e(x)$ and codebook latent variables e. The codebook variables are initialized from a normal distribution. By mapping all latent variables on a sphere, the Euclidean distance of ℓ_2-normalized latent variables $\|\ell_2(z_e(x)) - \ell_2(e_j)\|_2^2$ evolves to the cosine similarity of two vectors between $z_e(x)$ and e, further improving training stability and reconstruction quality shown in our experiments.

3.3 ViT-VQGAN Training Losses

We use a combination of logit-laplace loss, ℓ_2 loss, perceptual loss (Johnson et al., 2016; Zhang et al., 2018) based on VGG network (Simonyan & Zisserman, 2014) and GAN loss with architecture of StyleGAN discriminator (Karras et al., 2020). Loss balancing weights are configured with a hyper-parameter sweep to optimize image reconstruction quality, codebook usage, FID and Inception Score. After the sweep, we apply the same set of hyper-parameters of training losses to all datasets including CelebA-HQ, FFHQ, and ImageNet. Logit-Laplace loss can be viewed as normalized ℓ_1 loss which assumes the noise at the pixel level is laplace-distributed while ℓ_2 loss assumes

Model	Size	#Params	#Blocks	#Heads	Model Dim	Hidden Dim	Dropout	#Tokens
ViT-VQGAN	Small	32M	8	8	512	2048	0.0	1024
ViT-VQGAN	Base	91M	12	12	768	3072	0.0	1024
ViT-VQGAN	Large	599M	32	16	1280	5120	0.0	1024
VIM	Base	650M	24	16	1536	6144	0.1	1024
VIM	Large	1697M	36	32	2048	8192	0.1	1024

Table 2: Transformer architectures of Stage 1 ViT-VQGAN and Stage 2 VIM.

the noise is of a Gaussian distribution. We find logit-laplace loss contributes to codebook usage while ℓ_2 loss and perceptual loss significantly contribute to FID. The final loss combination we used by default is $L = L_{\text{VQ}} + 0.1\ L_{\text{Adv}} + 0.1\ L_{\text{Perceptual}} + 0.1\ L_{\text{Logit-laplace}} +\ 1.0 L_2$.

One caveat on the VGG-based perceptual loss is that the VGG network is pretrained with supervised classification loss, so the supervision might *leak* into Stage 2 for linear-probe accuracy measurement. Thus, for all of our reported unsupervised learning results, we exclude the perceptual loss during ViT-VQGAN training. For all unconditional and class-conditioned image synthesis, we use ViT-VQGAN quantizers trained with perceptual loss, as it leads to higher-fidelity reconstructions.

4 Vector-quantized Image Modeling

With a learned ViT-VQGAN, images are encoded into discrete latent code ids flattened in the raster order, similar to Image GPT (Chen et al., 2020a). A decoder-only Transformer model is used to model the density of image data $P(x)$ autoregressively as

$$P(x) = \prod_{i=1}^{n} P(x_i | x_1, x_2, ..., x_{i-1}; \theta), \tag{2}$$

where θ is learnable weights. The training objective is to minimize the negative log-likelihood of the data $L = \mathbb{E}_{x \in X}[-logP(x)]$.

Table 2 summarizes the architecture configurations for the Transformers. We first embed discrete image token ids into a learnable embedding space at each position, with an additive learnable 2D positional embedding. Both embedding dimensions are the same as model dimension. We apply a stack of Transformer blocks to the inputs with causal attention over the entire sequence. A dropout ratio of 0.1 is used in all residual, activation and attention outputs. At the final layer of all Transformer blocks, we apply an additional layer normalization.

4.1 Image Synthesis

With a pretrained generative Transformer model, unconditional image generation is achieved by simply sampling token-by-token from the output softmax distribution. All samples used for both qualitative and quantitative results are obtained without temperature reduction. The sampled tokens are then fed into the decoder of ViT-VQGAN to decode output images. Our default Stage 1 ViT-VQGAN encodes input images of resolution 256×256 into 32×32 latent codes with a codebook size 8192, while Stage 2 Transformer takes the flattened image tokens with total a length of 1024.

Class-conditioned ImageNet generation is also a widely used benchmark for measuring capabiltiy of models for image synthesis. We extend the unconditional generation to class-conditioned generation by prepending a class-id token before the image tokens. Separate embedding layers are learned from scratch for class-id token and image tokens, with the embedding dimension the same as the Transformer model dimension. During sampling, a class-id token is provided at the first position to decode the remaining image tokens autoregressively.

4.2 Unsupervised Learning

For the image understanding task, we feed all image tokens of the input into a pretrained Transformer, and get a sequence of 1024 token features. Similar to Image GPT (Chen et al., 2020a),

Model	Dataset	Latent Size	dim $\mathcal{Z}$	FID on Validation
DALL-E dVAE	Web data	32×32	8192	32.00
VQGAN	ImageNet	16×16	1024	7.94
VQGAN	ImageNet	16×16	16384	4.98
VQGAN*	ImageNet	32×32	8192	1.49
VQGAN**	ImageNet	64×64 & 32×32	512	1.45
ViT-VQGAN (Ours)	ImageNet	32×32	8192	1.28
ViT-VQGAN (Ours)	CelebA-HQ	32×32	8192	4.66
ViT-VQGAN (Ours)	FFHQ	32×32	8192	3.13

Table 3: Fréchet Inception Distance (FID) between reconstructed validation split and original validation split on ImageNet, CelebA-HQ and FFHQ. * denotes models trained with Gumbel-Softmax reparameterization as in Ramesh et al. (2021). ** denotes models trained with multi-scale hierarchical codebook as in Razavi et al. (2019).

we take a layer output at a specific block l over total blocks L, average over the sequence of token features (frozen) and insert a softmax layer (learnable) projecting averaged feature to class logits. We only take one specific Transformer block output instead of concatenating different block outputs as in iGPT (Chen et al., 2020a). We find that most discriminating feature for the linear-probe is typically near the middle of all Transformer blocks.

5 Experiments

5.1 Image Quantization

We train the proposed ViT-VQGAN on three datasets separately, CelebA-HQ (Karras et al., 2019), FFHQ (Karras et al., 2019), and ImageNet (Krizhevsky et al., 2012). For CelebA-HQ and FFHQ, we follow the default train and validation split as VQGAN (Esser et al., 2021).[1] For Stage 1 image quantization, three different architecture sizes are experimented, Small, Base and Large for either encoder or decoder, as defined in Table 2. The smallest ViT-VQGAN-SS has a Small-size encoder and Small-size decoder, while ViT-VQGAN-BB has a Base-size encoder and Base-size decoder. The largest ViT-VQGAN-SL has an asymmetric Small-size encoder and Large-size decoder, with the motivation that Stage 2 training only requires forward propagation of the encoder of ViT-VQGAN (in inference/decoding for image synthesis, the decoder of ViT-VQGAN is still required to decode images from codes predicted during Stage 2).

We train all ViT-VQGAN models with a training batch size of 256 distributed across 128 CloudTPUv4 for a total $500{,}000$ training steps. For both ViT-VQGAN and StyleGAN discriminator, Adam optimizer (Kingma & Ba, 2014) is used with $\beta_1 = 0.9$ and $\beta_2 = 0.99$ with the learning rate linearly warming up to a peak value of 1×10^{-4} over $50{,}000$ steps and then decaying to 5×10^{-5} over the remaining $450{,}000$ steps with a cosine schedule. We use a decoupled weight decay (Loshchilov & Hutter, 2017) of 1×10^{-4} for both ViT-VQGAN and StyleGAN discriminator. All models are trained with an input image resolution 256×256 on CloudTPUv4.

Table 3 shows FID between reconstructed images and original images in the validation split on ImageNet, CelebA-HQ and FFHQ datasets. Without multi-scale hierarchical codebook or gumbel-softmax, ViT-VQGAN is able to achieve better FID with a large codebook size of 8192 compared with vanilla VQGAN.

Table 4 provides extensive ablations on the proposed modifications, with empirical results on mean ℓ_1 distance, ℓ_2 distance, logit-laplace distance, Inception Score and FID on ImageNet. Among different model sizes, ViT-VQGAN-SS (small-encoder, small-decoder) performs worse than ViT-VQGAN-BB (base-encoder, base-decoder) and ViT-VQGAN-SL (small-encoder, large-decoder), but achieves much better throughput. The CNN-based VQGAN architecture is worse in both quality and throughput compared with ViT-based VQGAN. The StyleGAN-based discriminator (Karras et al., 2019) is more stable and yields better reconstruction quality than PatchGAN (Isola et al., 2017)

[1] https://github.com/CompVis/taming-transformers

Ablation on	Encoder Size	Decoder Size	Architecture	Discriminator	Latent dim	ℓ_2-normalized	ℓ_1 (1e-2) ↓	ℓ_2 (1e-3) ↓	Logit-Laplace ↓	IS ↑	FID ↓	Codebook Usage ↓	Throughput ↓
	Base	Base	ViT	StyleGAN	32	✓	3.06	3.09	-2.54	190.2	1.55	96%	960
Model Size	Small	Small	ViT	StyleGAN	32	✓	3.22	3.34	-2.44	184.4	1.99	95%	1520
	Small	Large	ViT	StyleGAN	32	✓	2.93	2.88	-2.58	192.3	1.28	95%	384
Architecture	-	-	CNN	StyleGAN	32	✓	3.45	3.81	-2.36	178.7	2.26	63%	946
	Base	Base	ViT	PatchGAN	32	✓	2.82	2.58	-2.62	165.6	3.88	89%	1227
Codebook Learning	Base	Base	ViT	StyleGAN	256	✓	3.60	4.28	-2.38	160.1	3.68	4%	954
	Base	Base	ViT	StyleGAN	128	✓	3.41	3.93	-2.44	173.9	2.77	14%	960
	Base	Base	ViT	StyleGAN	64	✓	3.18	3.37	-2.49	179.5	2.50	37%	960
	Base	Base	ViT	StyleGAN	16	✓	3.00	2.96	-2.54	191.2	1.50	95%	960
	Base	Base	ViT	StyleGAN	8	✓	2.98	2.92	-2.55	189.5	1.52	96%	960
	Base	Base	ViT	StyleGAN	4	✓	3.55	4.18	-2.37	143.8	3.68	96%	960
	Base	Base	ViT	StyleGAN	32	✗	4.13	5.41	-2.20	123.6	5.44	2%	960

Table 4: Ablation study on ViT-VQGAN. The codebook usage is calculated as the percentage of used codes given a batch of 256 test images averaged over the entire test set.

CelebA-HQ 256 × 256		FFHQ 256 × 256	
Method	FID ↓	Method	FID ↓
GLOW (Kingma & Dhariwal, 2018)	69.0	VDVAE ($t = 0.7$) (Child, 2021)	38.8
NVAE (Vahdat & Kautz, 2020)	40.3	VDVAE ($t = 1.0$)	33.5
PIONEER (Heljakka et al., 2018)	25.3	VDVAE ($t = 0.8$)	29.8
NCPVAE (Aneja et al., 2020)	24.8	VDVAE ($t = 0.9$)	28.5
VAEBM (Xiao et al., 2021)	20.4	*VQGAN*+P.SNAIL	21.9
Style ALAE (Pidhorskyi et al., 2020)	19.2	BigGAN	12.4
DC-VAE (Parmar et al., 2021)	15.8	U-Net GAN (Schonfeld et al., 2020)	10.9
PGGAN (Karras et al., 2018)	8.0	StyleGAN2 (Karras et al., 2020)	3.8
VQGAN (w/ top-k sampling)	10.2	VQGAN (w/ top-k sampling)	9.6
ViT-VQGAN (Ours)	7.0	**ViT-VQGAN (Ours)**	5.3

Table 5: FID comparison with unconditional image synthesis on CelebA-HQ and FFHQ.

(which was used for VQGAN). For codebook learning, factorized codes with low-dimensional latent variables consistently achieve better reconstruction quality when the latent dimension is reduced from 256 to 16 or 8. Moreover, removing ℓ_2-normalization leads to much worse results.

5.2 Image Synthesis

On top of the pre-learned ViT-VQGAN image quantizer, we train stage 2 transformer models for unconditional and class-conditioned image synthesis and compare with previous work. We use a default model size of ViT-VQGAN-SS (small-encoder, small-decoder) for stage 1 and VIM-Large for stage 2 (model architectures are listed in Table 2), as we find it beneficial to put more computation in stage 2 while keeping stage 1 transformers lightweight. We also present a model size ablation study and comparison with VQGAN in the Appendix. Models are trained with a global training batch size of 1024 for a total of 450,000 training steps. We use Adam optimizer (Kingma & Ba, 2014) with $\beta_1 = 0.9$ and $\beta_2 = 0.96$ with the learning rate linearly warming up to a peak constant value of 4.5×10^{-4} over the first 5000 steps and then exponentially decaying to 1×10^{-5} starting from 80,000 steps. To save memory, we use a factorized version of Adam, Adafactor (Shazeer & Stern, 2018), with the first moment quantized into Int8 and factorized second moments. No other techniques like mixed-precision training, model sharding, or gradient compression is used. All models are trained with an input image resolution 256×256 on CloudTPUv4.

Model	Acceptance Rate	FID	IS
Validation data	1.0	1.62	235.0
DCTransformer (Nash et al., 2021)	1.0	36.5	n/a
BigGAN (Brock et al., 2019)	1.0	7.53	168.6
BigGAN-deep	1.0	6.84	203.6
IDDPM (Nichol & Dhariwal, 2021)	1.0	12.3	n/a
ADM-G, no guid. (Dhariwal & Nichol, 2021)	1.0	10.94	101.0
ADM-G, 1.0 guid.	1.0	4.59	186.7
VQVAE-2 (Razavi et al., 2019)	1.0	$\sim$31	$\sim$45
VQGAN (Esser et al., 2021)	1.0	17.04	70.6
VQGAN	0.5	10.26	125.5
VQGAN	0.25	7.35	188.6
ViT-VQGAN (Ours)	1.0	4.17	175.1
ViT-VQGAN (Ours)	0.5	3.04	227.4

Table 6: FID comparison for class-conditional image synthesis on ImageNet with resolution 256 × 256. Acceptance rate shows results based on ResNet-101 classifier-based rejection sampling.

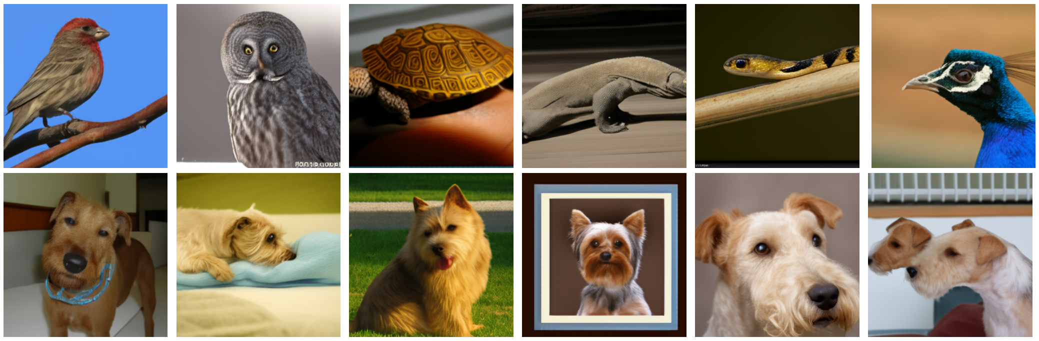

Figure 2: Uncurated set of samples from class-conditioned image generation trained on ImageNet. Top row shows sampled class ids while bottom row shows fine-grained dog species from class id 184 to 189. More samples are shown in Appendix.

Our main results on unconditional image synthesis on CelebA-HQ and FFHQ are summarized in Table 5. Without top-k and top-p (nucleus) sampling heuristics, we achieve FID of 7.0 on CelebA-HQ and 5.3 on FFHQ, significantly better than VQGAN (Esser et al., 2021). Table 6 shows class-conditioned image synthesis models on ImageNet, following Section 4.1. Based on ViT-VQGAN-SS, we achieve IS of 175.1 and FID of 4.17, improving over the IS of 70.6 and FID of 17.04 with vanilla VQGAN. When applied with classifier-based rejection sampling, the ViT-VQGAN based model further achieves best FID of 3.04 and best Inception Score of 321.7. Qualitative results are sampled and shown in Figure 2 (see the Appendix for more).

5.3 Unsupervised Learning

After the generative pretraining to autoregressively model the density of ViT-VQGAN quantized image tokens, we evaluate the learned representation under the common linear protocol on ImageNet classification. We follow the same training hyper-parameters as the unconditional image synthesis models on ImageNet, and use ViT-VQGAN-SS image quantizer for better training throughput. As discussed in Section 3.3, the ViT-VQGAN-SS image quantizer is trained without perceptual loss for unsupervised learning (perceptual loss is based on a supervised VGG network trained on ImageNet, which may make comparison unfair). We apply an average pooling over the token features at a specific transformer block l from totally L blocks. Similar to findings reported in iGPT (Chen et al., 2020a), the representations from the middle transformer blocks has better linear-probe accuracy (more study can be found in Appendix). Specifically, we use the Transformer block of index 15 (36 blocks in total) for VIM-Large and index 10 (24 blocks in total) for VIM-Base (architecture configurations are listed in Table 2).

	Method	#Tokens	Features	Params	Top-1 ↑
Discriminative Pretraining	Jigsaw (Noroozi & Favaro, 2016b)	-	4096	94M	44.6
	RelativePosition (Doersch et al., 2015)	-	4096	94M	51.4
	Rotation (Gidaris et al., 2018b)	-	8192	86M	55.4
	AMDIM (Bachman et al., 2019)	-	8192	626M	68.1
	CPC v2 (Henaff, 2020)	-	4096	303M	71.5
	MoCo (He et al., 2020)	-	8192	375M	68.6
	SimCLR (Chen et al., 2020b)	-	8192	375M	76.5
	SwAV (Caron et al., 2020)	-	2048	93M	75.3
	DINO (Caron et al., 2021)	-	2048	85M	75.3
	BYOL (Grill et al., 2020)	-	8192	375M	78.6
Generative Pretraining	BiGAN (Donahue et al., 2016)	-	512	138M	31.0
	BigBiGAN (Donahue & Simonyan, 2019b)	-	4096	86M	56.6
	BigBiGAN	-	16384	344M	61.3
	iGPT-L (Chen et al., 2020a)	32 × 32	1536	1362M	60.3
	iGPT-L	48 × 48	1536	1362M	65.2
	iGPT-XL (extra data)	64 × 64	3072	6801M	68.7
	iGPT-XL (extra data, feature ensemble)	64 × 64	5 × 3072	6801M	72.0
	VIM-Base (Ours)	32 × 32	1024	650M	65.1
	VIM-Large (Ours)	32 × 32	2048	1697M	73.2
	VIM-Base + DALL-E dVAE quantizer	32 × 32	1024	650M	63.8 (-1.3)
	VIM-Base + CNN-VQGAN quantizer	32 × 32	1024	650M	61.8 (-3.3)

Table 7: Linear-probe accuracy with different unsupervised learning methods on ImageNet. DALL-E dVAE (Ramesh et al., 2021) image quantizer is trained with extra image data. VIM-Large is trained without dropout in transformers.

Table 7 shows the comparisons among different approaches divided into two categories: discriminative pretraining methods to distinguish among cropped or augmented image patches; and generative pretraining methods to generate image pixels or patches. The linear-probe accuracy of our proposed VIM with ViT-VQGAN are superior to other generative pretraining approaches like iGPT, and competitive with discriminative pretraining methods like BYOL (Grill et al., 2020) and DINO (Caron et al., 2021). Specifically, ImageNet-pretrained VIM-L significantly improves over iGPT-L, increasing linear-probe accuracy from 60.3% to 73.2% for a similar model size. VIM-L also outperforms iGPT-XL, which is larger and trained with extra web image data. Moreover, we also compare different stage 1 quantizers including CNN-based VQGAN and pretrained DALL-E dVAE (trained with extra web-scale image data)[2] in Table 7; these results are all worse than ViT-VQGAN quantizer, suggesting the importance of the multiple changes defined in Section 3.

6 Ethics

Tasks involving generation raise a number of issues that should be considered, such as possible biases in underlying models and data—especially with respect to capabilities for people with different demographic backgrounds. The three datasets used in this paper–ImageNet, CelebA-HQ, and FFHQ–are all widely used in the literature, but it is worthwhile highlighting their unique natures and recent scholarship around them.

The FFHQ dataset[3] contains 70,000 images collected from Flickr, all of which have licenses appropriate for sharing, and the data maintainers provide means for individuals to opt-out of inclusion in the dataset. FFHQ was specifically collected to cover a broad range of demographics with respect to faces of people. This is confirmed in our models' generated examples, which cover a broad range of perceived ages, genders and ethnicities. Nevertheless, Balakrishnan et al. (2020) provide an extensive analysis of multiple forms of bias in datasets (including CelebA-HQ and FFHQ) and algorithms for face generation; not only do they find imbalances in skin tone in FFHQ, but also correlations between multiple attributes such as skin tone and hair length. Based on this and other

[2] https://github.com/openai/dall-e

[3] `https://github.com/NVlabs/ffhq-dataset`

factors such as privacy and copyright, they argue that synthetically-created face datasets, for which multiple attributes can be controlled, is an important direction of investment and general inquiry.

The CelebA-HQ dataset covers celebrities, which brings a consequent bias toward images of attractive people who are mostly in age range of twenty to forty years old. Esser et al. (2020) discusses these biases in details, and they furthermore project images from the FFHQ dataset onto CelebA-HQ: the main effect of which is to produce images of younger people with features conforming more to norms of celebrities popular in the United States of America. Our model's generations appear to have a similar bias as derived from training on CelebA-HQ. Neverethless, they do show broad coverage of different perceived genders and ethnicities, but with age skewed to the 20-40 year old range.

ImageNet is, of course, quite pervasive in computer vision. In this paper, we learn to generate images given ImageNet class labels; these labels mostly concern animals, plants and things. People are sometimes generated when conditioning on classes such as `sunglasses` since the training data images contain people wearing sunglasses, but the generated images contain few depictions of people overall. Nevertheless, it is important to recognize that ImageNet itself was created with biases in terms of image selection and label annotation as a result of its process of creation (Denton et al., 2021). Given this, results present on ImageNet cover a significant, but nonetheless biased, sample of the kinds of scenes and objects one might encounter across the entire world.

There are also potential problematic aspects of image generation models, as demonstrated with biases found in the PULSE model (Menon et al., 2020) (see Section 6) and in model correlations with human biases found in social psychology (Steed & Caliskan, 2021), as well as with possible uses of such models to create fake media (Westerlund, 2019).

REFERENCES

Jyoti Aneja, Alexander G. Schwing, Jan Kautz, and Arash Vahdat. NCP-VAE: variational autoencoders with noise contrastive priors. *CoRR*, abs/2010.02917, 2020. URL `https://arxiv.org/abs/2010.02917`.

Philip Bachman, R Devon Hjelm, and William Buchwalter. Learning representations by maximizing mutual information across views. *arXiv preprint arXiv:1906.00910*, 2019.

Guha Balakrishnan, Yuanjun Xiong, Wei Xia, and Pietro Perona. Towards causal benchmarking of bias in face analysis algorithms, 2020.

Hangbo Bao, Li Dong, and Furu Wei. Beit: BERT pre-training of image transformers. *arXiv preprint arXiv:2106.08254*, 2021.

Andrew Brock, Jeff Donahue, and Karen Simonyan. Large scale gan training for high fidelity natural image synthesis. In *ICLR*, 2019.

Tom B Brown, Benjamin Mann, Nick Ryder, Melanie Subbiah, Jared Kaplan, Prafulla Dhariwal, Arvind Neelakantan, Pranav Shyam, Girish Sastry, Amanda Askell, et al. Language models are few-shot learners. *arXiv preprint arXiv:2005.14165*, 2020.

Mathilde Caron, Ishan Misra, Julien Mairal, Priya Goyal, Piotr Bojanowski, and Armand Joulin. Unsupervised learning of visual features by contrasting cluster assignments. *arXiv preprint arXiv:2006.09882*, 2020.

Mathilde Caron, Hugo Touvron, Ishan Misra, Hervé Jégou, Julien Mairal, Piotr Bojanowski, and Armand Joulin. Emerging properties in self-supervised vision transformers. *arXiv preprint arXiv:2104.14294*, 2021.

Mark Chen, Alec Radford, Rewon Child, Jeffrey Wu, Heewoo Jun, David Luan, and Ilya Sutskever. Generative pretraining from pixels. In *International Conference on Machine Learning*, pp. 1691–1703. PMLR, 2020a.

Ting Chen, Simon Kornblith, Mohammad Norouzi, and Geoffrey Hinton. A simple framework for contrastive learning of visual representations. In *International conference on machine learning*, pp. 1597–1607. PMLR, 2020b.

Ting Chen, Simon Kornblith, Kevin Swersky, Mohammad Norouzi, and Geoffrey Hinton. Big self-supervised models are strong semi-supervised learners. *arXiv preprint arXiv:2006.10029*, 2020c.

Xi Chen, Nikhil Mishra, Mostafa Rohaninejad, and Pieter Abbeel. Pixelsnail: An improved autoregressive generative model. In Jennifer G. Dy and Andreas Krause (eds.), *ICML*, 2018.

Xinlei Chen, Haoqi Fan, Ross Girshick, and Kaiming He. Improved baselines with momentum contrastive learning. *arXiv preprint arXiv:2003.04297*, 2020d.

Rewon Child. Very deep {vae}s generalize autoregressive models and can outperform them on images. In *International Conference on Learning Representations*, 2021. URL `https://openreview.net/forum?id=RLRXCV6DbEJ`.

Andrew M Dai and Quoc V Le. Semi-supervised sequence learning. *Advances in neural information processing systems*, 28:3079–3087, 2015.

Emily Denton, Alex Hanna, Razvan Amironesei, Andrew Smart, and Hilary Nicole. On the genealogy of machine learning datasets: A critical history of imagenet. *Big Data & Society*, 8(2): 20539517211035955, 2021. doi: 10.1177/20539517211035955. URL `https://doi.org/10.1177/20539517211035955`.

Jacob Devlin, Ming-Wei Chang, Kenton Lee, and Kristina Toutanova. BERT: pre-training of deep bidirectional transformers for language understanding. In Jill Burstein, Christy Doran, and Thamar Solorio (eds.), *NAACL-HLT*, 2019.

Prafulla Dhariwal and Alex Nichol. Diffusion models beat gans on image synthesis. *arXiv preprint arXiv:2105.05233*, 2021.

Carl Doersch, Abhinav Gupta, and Alexei A Efros. Unsupervised visual representation learning by context prediction. In *Proceedings of the IEEE international conference on computer vision*, pp. 1422–1430, 2015.

Jeff Donahue and Karen Simonyan. Large scale adversarial representation learning. In Hanna M. Wallach, Hugo Larochelle, Alina Beygelzimer, Florence d'Alché-Buc, Emily B. Fox, and Roman Garnett (eds.), *NeurIPS*, 2019a.

Jeff Donahue and Karen Simonyan. Large scale adversarial representation learning. *arXiv preprint arXiv:1907.02544*, 2019b.

Jeff Donahue, Philipp Krähenbühl, and Trevor Darrell. Adversarial feature learning. *arXiv preprint arXiv:1605.09782*, 2016.

Jeff Donahue, Philipp Krähenbühl, and Trevor Darrell. Adversarial feature learning. In *ICLR*, 2017.

Alexey Dosovitskiy, Lucas Beyer, Alexander Kolesnikov, Dirk Weissenborn, Xiaohua Zhai, Thomas Unterthiner, Mostafa Dehghani, Matthias Minderer, Georg Heigold, Sylvain Gelly, et al. An image is worth 16x16 words: Transformers for image recognition at scale. *arXiv preprint arXiv:2010.11929*, 2020.

Patrick Esser, Robin Rombach, and Björn Ommer. A note on data biases in generative models. In *NeurIPS 2020 Workshop on Machine Learning for Creativity and Design*, 2020. URL `https://arxiv.org/abs/2012.02516`.

Patrick Esser, Robin Rombach, and Björn Ommer. Taming transformers for high-resolution image synthesis. In *CVPR*, 2021.

Spyros Gidaris, Praveer Singh, and Nikos Komodakis. Unsupervised representation learning by predicting image rotations. In *ICLR*, 2018a.

Spyros Gidaris, Praveer Singh, and Nikos Komodakis. Unsupervised representation learning by predicting image rotations. *arXiv preprint arXiv:1803.07728*, 2018b.

Ian J. Goodfellow, Jean Pouget-Abadie, Mehdi Mirza, Bing Xu, David Warde-Farley, Sherjil Ozair, Aaron C. Courville, and Yoshua Bengio. Generative adversarial nets. In *NeurIPS*, 2014.

Jean-Bastien Grill, Florian Strub, Florent Altché, Corentin Tallec, Pierre H Richemond, Elena Buchatskaya, Carl Doersch, Bernardo Avila Pires, Zhaohan Daniel Guo, Mohammad Gheshlaghi Azar, et al. Bootstrap your own latent: A new approach to self-supervised learning. *arXiv preprint arXiv:2006.07733*, 2020.

Kaiming He, Haoqi Fan, Yuxin Wu, Saining Xie, and Ross Girshick. Momentum contrast for unsupervised visual representation learning. In *Proceedings of the IEEE/CVF Conference on Computer Vision and Pattern Recognition*, pp. 9729–9738, 2020.

Ari Heljakka, Arno Solin, and Juho Kannala. Pioneer networks: Progressively growing generative autoencoder. In *Asia conference on computer vision*, 2018.

Olivier Henaff. Data-efficient image recognition with contrastive predictive coding. In *International Conference on Machine Learning*, pp. 4182–4192. PMLR, 2020.

Irina Higgins, Loïc Matthey, Arka Pal, Christopher Burgess, Xavier Glorot, Matthew Botvinick, Shakir Mohamed, and Alexander Lerchner. beta-vae: Learning basic visual concepts with a constrained variational framework. In *ICLR*, 2017.

Ari Holtzman, Jan Buys, Li Du, Maxwell Forbes, and Yejin Choi. The curious case of neural text degeneration. In *International Conference on Learning Representations*, 2020. URL https://openreview.net/forum?id=rygGQyrFvH.

Phillip Isola, Jun-Yan Zhu, Tinghui Zhou, and Alexei A. Efros. Image-to-image translation with conditional adversarial networks. In *2017 IEEE Conference on Computer Vision and Pattern Recognition (CVPR)*, pp. 5967–5976, 2017. doi: 10.1109/CVPR.2017.632.

Justin Johnson, Alexandre Alahi, and Li Fei-Fei. Perceptual losses for real-time style transfer and super-resolution. In *European conference on computer vision*, pp. 694–711. Springer, 2016.

Tero Karras, Timo Aila, Samuli Laine, and Jaakko Lehtinen. Progressive growing of GANs for improved quality, stability, and variation. In *International Conference on Learning Representations*, 2018. URL https://openreview.net/forum?id=Hk99zCeAb.

Tero Karras, Samuli Laine, and Timo Aila. A style-based generator architecture for generative adversarial networks. In *Proceedings of the IEEE/CVF Conference on Computer Vision and Pattern Recognition (CVPR)*, June 2019.

Tero Karras, Samuli Laine, Miika Aittala, Janne Hellsten, Jaakko Lehtinen, and Timo Aila. Analyzing and improving the image quality of stylegan. In *Proceedings of the IEEE/CVF Conference on Computer Vision and Pattern Recognition*, pp. 8110–8119, 2020.

Diederik P Kingma and Jimmy Ba. Adam: A method for stochastic optimization. *arXiv preprint arXiv:1412.6980*, 2014.

Diederik P. Kingma and Max Welling. Auto-encoding variational bayes. In *ICLR*, 2014.

Durk P Kingma and Prafulla Dhariwal. Glow: Generative flow with invertible 1x1 convolutions. In S. Bengio, H. Wallach, H. Larochelle, K. Grauman, N. Cesa-Bianchi, and R. Garnett (eds.), *Advances in Neural Information Processing Systems*, volume 31. Curran Associates, Inc., 2018. URL https://proceedings.neurips.cc/paper/2018/file/d139db6a236200b21cc7f752979132d0-Paper.pdf.

Alex Krizhevsky, Ilya Sutskever, and Geoffrey E Hinton. Imagenet classification with deep convolutional neural networks. *Advances in neural information processing systems*, 25:1097–1105, 2012.

Julia A Lasserre, Christopher M Bishop, and Thomas P Minka. Principled hybrids of generative and discriminative models. In *2006 IEEE Computer Society Conference on Computer Vision and Pattern Recognition (CVPR'06)*, volume 1, pp. 87–94. IEEE, 2006.

Ilya Loshchilov and Frank Hutter. Decoupled weight decay regularization. *arXiv preprint arXiv:1711.05101*, 2017.

Sachit Menon, Alex Damian, McCourt Hu, Nikhil Ravi, and Cynthia Rudin. Pulse: Self-supervised photo upsampling via latent space exploration of generative models. In *The IEEE Conference on Computer Vision and Pattern Recognition (CVPR)*, June 2020.

Charlie Nash, Jacob Menick, S. Dieleman, and P. Battaglia. Generating images with sparse representations. *ICML*, abs/2103.03841, 2021.

Alexander Quinn Nichol and Prafulla Dhariwal. Improved denoising diffusion probabilistic models. In Marina Meila and Tong Zhang (eds.), *Proceedings of the 38th International Conference on Machine Learning*, volume 139 of *Proceedings of Machine Learning Research*, pp. 8162–8171. PMLR, 18–24 Jul 2021. URL `https://proceedings.mlr.press/v139/nichol21a.html`.

Mehdi Noroozi and Paolo Favaro. Unsupervised learning of visual representations by solving jigsaw puzzles. In Bastian Leibe, Jiri Matas, Nicu Sebe, and Max Welling (eds.), *ECCV*, 2016a.

Mehdi Noroozi and Paolo Favaro. Unsupervised learning of visual representations by solving jigsaw puzzles. In *European conference on computer vision*, pp. 69–84. Springer, 2016b.

Aaron van den Oord, Oriol Vinyals, and Koray Kavukcuoglu. Neural discrete representation learning. *arXiv preprint arXiv:1711.00937*, 2017.

Gaurav Parmar, Dacheng Li, Kwonjoon Lee, and Zhuowen Tu. Dual contradistinctive generative autoencoder. In *Proceedings of the IEEE/CVF Conference on Computer Vision and Pattern Recognition (CVPR)*, pp. 823–832, June 2021.

Niki Parmar, Ashish Vaswani, Jakob Uszkoreit, Lukasz Kaiser, Noam Shazeer, Alexander Ku, and Dustin Tran. Image transformer. In Jennifer G. Dy and Andreas Krause (eds.), *ICML*, 2018.

Stanislav Pidhorskyi, Donald A Adjeroh, and Gianfranco Doretto. Adversarial latent autoencoders. In *Proceedings of the IEEE Computer Society Conference on Computer Vision and Pattern Recognition (CVPR)*, 2020. [to appear].

Alec Radford, Luke Metz, and Soumith Chintala. Unsupervised representation learning with deep convolutional generative adversarial networks. In Yoshua Bengio and Yann LeCun (eds.), *ICLR*, 2016.

Alec Radford, Karthik Narasimhan, Tim Salimans, and Ilya Sutskever. Improving language understanding by generative pre-training. 2018.

Alec Radford, Jeffrey Wu, Rewon Child, David Luan, Dario Amodei, Ilya Sutskever, et al. Language models are unsupervised multitask learners. *OpenAI blog*, 1(8):9, 2019.

Aditya Ramesh, Mikhail Pavlov, Gabriel Goh, Scott Gray, Chelsea Voss, Alec Radford, Mark Chen, and Ilya Sutskever. Zero-shot text-to-image generation. In Marina Meila and Tong Zhang (eds.), *ICML*, 2021.

Ali Razavi, Aäron van den Oord, and Oriol Vinyals. Generating diverse high-fidelity images with VQ-VAE-2. In Hanna M. Wallach, Hugo Larochelle, Alina Beygelzimer, Florence d'Alché-Buc, Emily B. Fox, and Roman Garnett (eds.), *NeurIPS*, 2019.

Edgar Schonfeld, Bernt Schiele, and Anna Khoreva. A u-net based discriminator for generative adversarial networks. In *Proceedings of the IEEE/CVF Conference on Computer Vision and Pattern Recognition*, pp. 8207–8216, 2020.

Noam Shazeer and Mitchell Stern. Adafactor: Adaptive learning rates with sublinear memory cost. In *International Conference on Machine Learning*, pp. 4596–4604. PMLR, 2018.

Karen Simonyan and Andrew Zisserman. Very deep convolutional networks for large-scale image recognition. *arXiv preprint arXiv:1409.1556*, 2014.

Yang Song and Stefano Ermon. Generative modeling by estimating gradients of the data distribution. In Hanna M. Wallach, Hugo Larochelle, Alina Beygelzimer, Florence d'Alché-Buc, Emily B. Fox, and Roman Garnett (eds.), *NeurIPS*, 2019.

Ryan Steed and Aylin Caliskan. Image representations learned with unsupervised pre-training contain human-like biases. In *The 2021 ACM Conference on Fairness, Accountability, and Transparency (ACM FAccT 2021)*, 2021. URL `https://arxiv.org/abs/2010.15052`.

Arash Vahdat and Jan Kautz. NVAE: A deep hierarchical variational autoencoder. In Hugo Larochelle, Marc'Aurelio Ranzato, Raia Hadsell, Maria-Florina Balcan, and Hsuan-Tien Lin (eds.), *NeurIPS*, 2020.

Aäron van den Oord, Nal Kalchbrenner, Lasse Espeholt, Koray Kavukcuoglu, Oriol Vinyals, and Alex Graves. Conditional image generation with pixelcnn decoders. In Daniel D. Lee, Masashi Sugiyama, Ulrike von Luxburg, Isabelle Guyon, and Roman Garnett (eds.), *NeurIPS*, 2016.

Aäron van den Oord, Oriol Vinyals, and Koray Kavukcuoglu. Neural discrete representation learning. In Isabelle Guyon, Ulrike von Luxburg, Samy Bengio, Hanna M. Wallach, Rob Fergus, S. V. N. Vishwanathan, and Roman Garnett (eds.), *NeurIPS*, 2017.

Aäron van den Oord, Yazhe Li, and Oriol Vinyals. Representation learning with contrastive predictive coding. *arXiv preprint arXiv:1807.03748*, abs/1807.03748, 2018.

Ashish Vaswani, Noam Shazeer, Niki Parmar, Jakob Uszkoreit, Llion Jones, Aidan N. Gomez, Lukasz Kaiser, and Illia Polosukhin. Attention is all you need. In *NeurIPS*, 2017.

Mika Westerlund. The emergence of deepfake technology: A review. *Technology Innovation Management Review*, 9:40–53, 11/2019 2019. ISSN 1927-0321. doi: http://doi.org/10.22215/timreview/1282. URL `timreview.ca/article/1282`.

Zhisheng Xiao, Karsten Kreis, Jan Kautz, and Arash Vahdat. {VAEBM}: A symbiosis between variational autoencoders and energy-based models. In *International Conference on Learning Representations*, 2021. URL `https://openreview.net/forum?id=5m3SEczOV8L`.

Han Zhang, Ian Goodfellow, Dimitris Metaxas, and Augustus Odena. Self-attention generative adversarial networks. In *International conference on machine learning*, pp. 7354–7363. PMLR, 2019a.

Han Zhang, Ian J. Goodfellow, Dimitris N. Metaxas, and Augustus Odena. Self-attention generative adversarial networks. In *ICML*, 2019b.

Richard Zhang, Phillip Isola, Alexei A Efros, Eli Shechtman, and Oliver Wang. The unreasonable effectiveness of deep features as a perceptual metric. In *Proceedings of the IEEE conference on computer vision and pattern recognition*, pp. 586–595, 2018.

A LINEAR-PROBE ON IMAGENET

We show linear-probe accuracy from different layers in a pretrained VIM-Base Transformer model in Figure 3. Similar to iGPT (Chen et al., 2020a), we also find the last few layers may not be the best layers for discriminative features, as the generative pretraining objective is to recover the original image tokens. The linear-probe accuracy increases quickly from the first transformer output, reaches its peak at middle layers, and finally decreases for the last few blocks. Interestingly, we find for both VIM-Base and VIM-Large, the middle transformer block has the near-best result. This observation connects the transformer model to an encoder-decoder model where the encoder encodes image tokens into high-level semantic features and the decoder takes feature information to generate output image tokens. We leave for future study regrading the interpretability of pretrained VIM models.

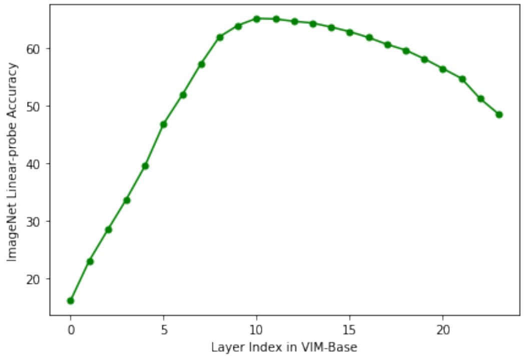

Figure 3: Linear-probe accuracy from different layers in a pretrained VIM-Base Transformer model.

B Model Sizes of Class-conditioned ImageNet Synthesis

We also present results of different sizes of Stage 2 Transformers for class-conditioned image synthesis and compare with VQGAN (Esser et al., 2021)[4] summarized in Table 8.

Model	Stage-2 Transformer Size	#Tokens	FID	IS
Validation data	-	-	1.62	235.0
VQGAN (Esser et al., 2021)	1.4B	16 × 16	17.04	70.6
ViT-VQGAN + VIM-Base	650M	16 × 16	11.20	97.2
ViT-VQGAN + VIM-Large	1.7B	16 × 16	5.3	149.9
ViT-VQGAN + VIM-Base	650M	32 × 32	8.81	110.8
ViT-VQGAN + VIM-Large	1.7B	32 × 32	4.17	175.1

Table 8: FID comparison for class-conditional image synthesis on ImageNet with different Transformer sizes in Stage 2. Results are reported without rejection sampling.

C Implementation Details of Factorized Codebook

As we introduced in Section 3.2, we use a linear projection to reduce the encoded embedding to a low-dimensional variable space for code lookup. A detailed illustration is shown in Figure 4.

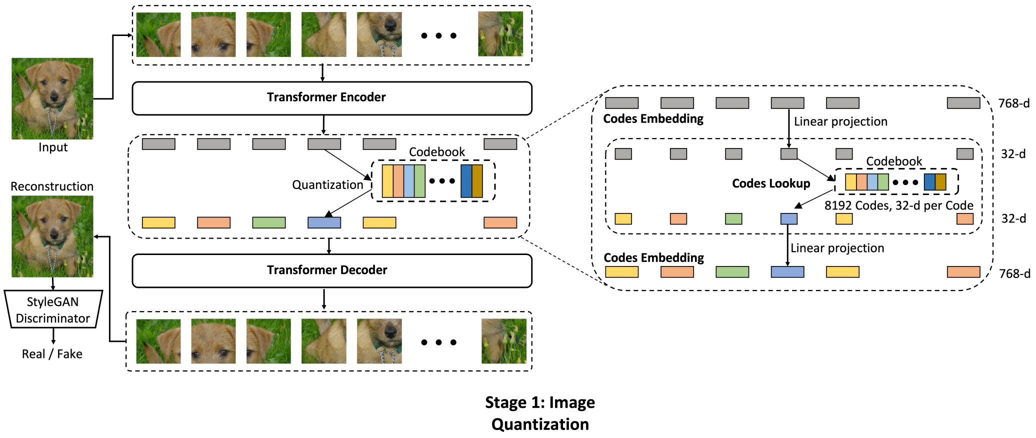

Figure 4: Illustration of factorized codes and codebook details.

D More Samples on Class-conditioned ImageNet Synthesis

[4] https://github.com/CompVis/taming-transformers

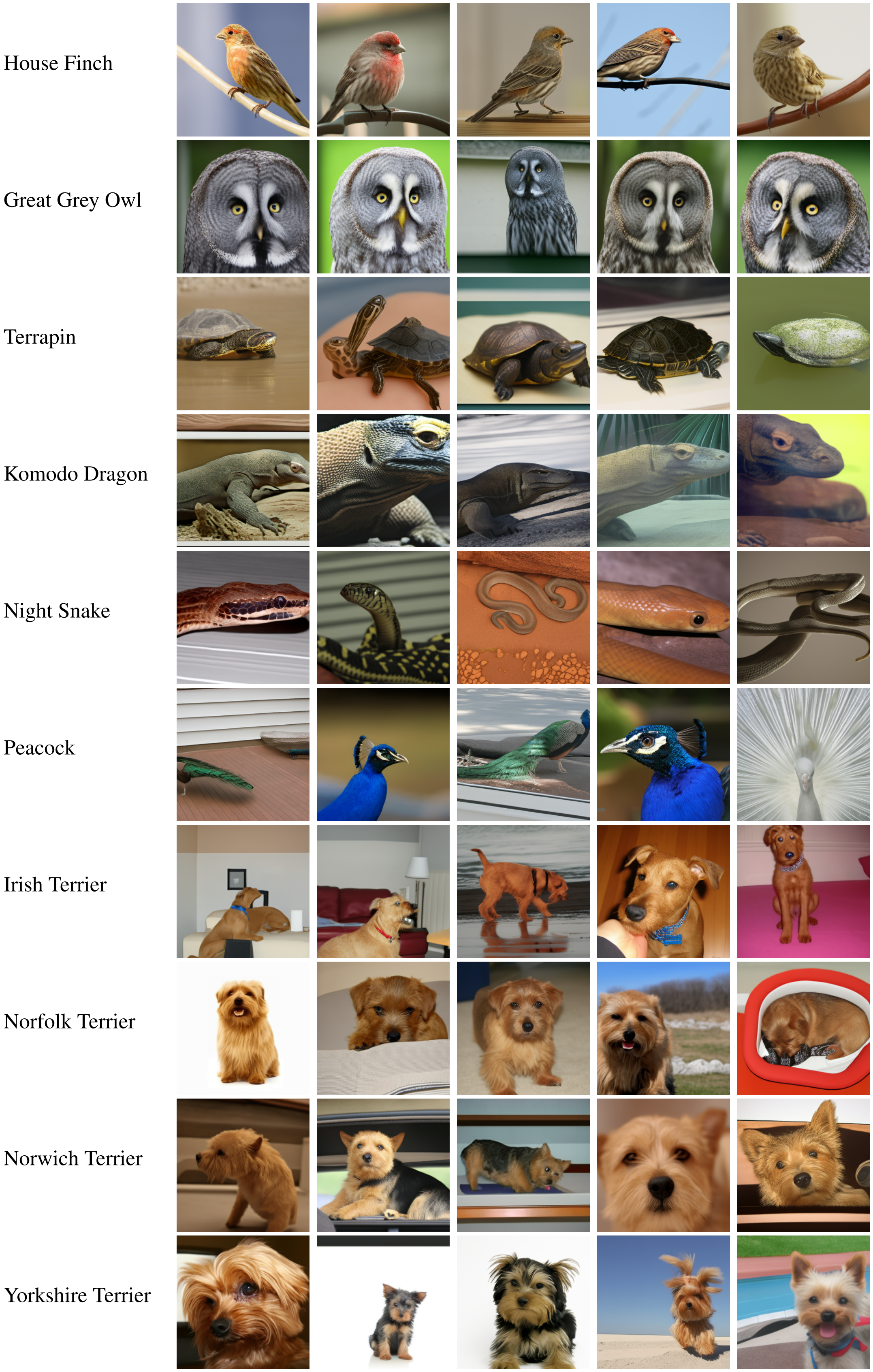

Figure 5: Uncurated set of samples from class-conditioned generation trained on ImageNet.

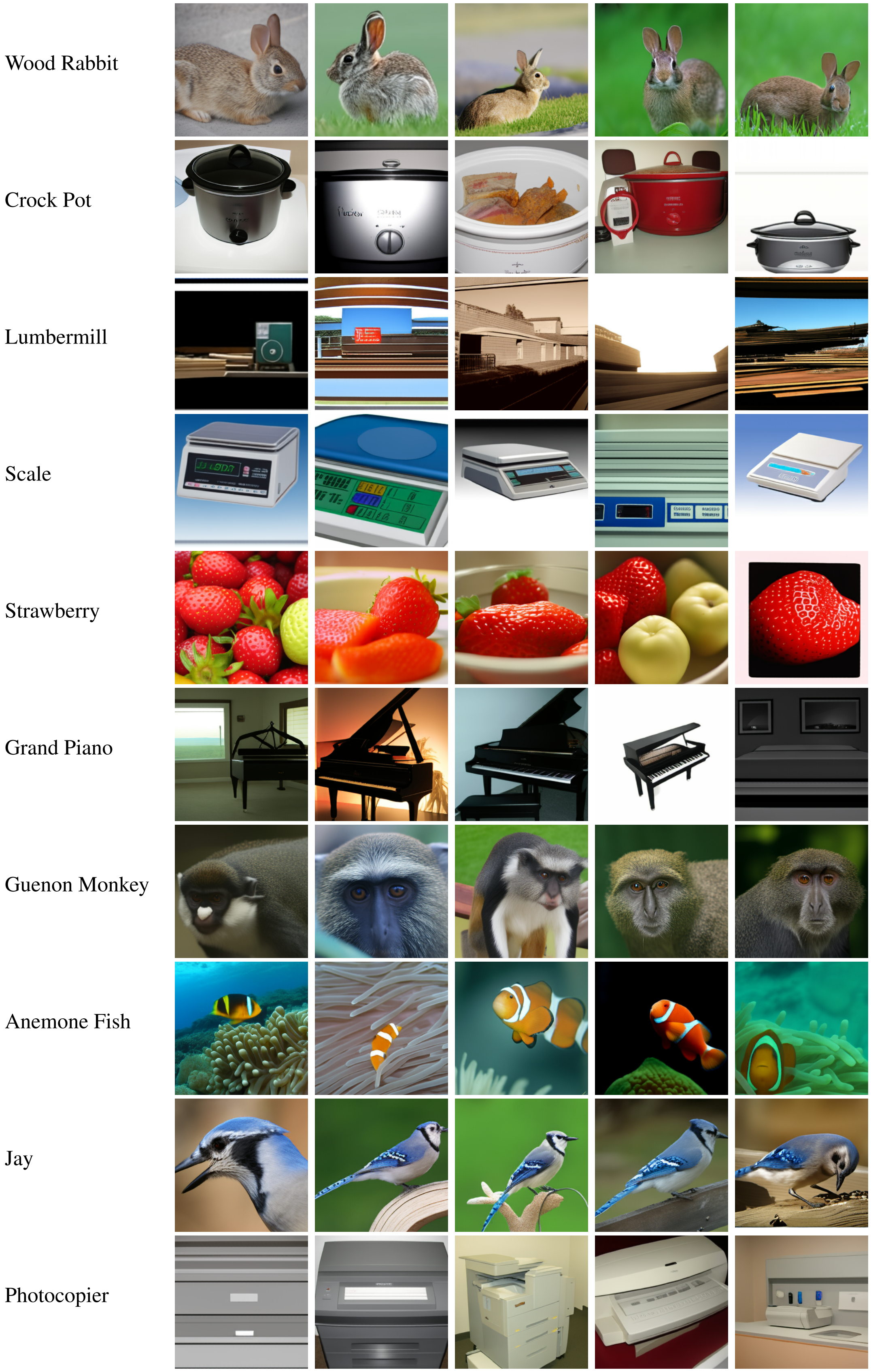

Figure 6: Uncurated set of samples from class-conditioned generation trained on ImageNet.